Macromolecules
ARTICLE
pubs.acs.org/Macromolecules

Effects of Si−O−Si Agglomerations on CO_2 Transport and Separation Properties of Sol-Derived Nanohybrid Membranes

Cher Hon Lau and Tai-Shung Chung*

Department of Chemical & Biomolecular Engineering, National University of Singapore, 4 Engineering Drive 4, 117576 Singapore

ABSTRACT: Nanohybrid membranes comprising organic and inorganic components with high CO_2 affinity are ideal substitutes for traditional high footprint gas separation technologies. The CO_2 permeability of these membranes resembles those of polydimethylsiloxane (PDMS), the most permeable rubbery material, while possessing CO_2/H_2 separation factors that supersede PDMS. Such membranes are synthesized using a simple acid-catalyzed sol−gel process. In this work, we investigate the relationship between the CO_2 permeation properties of these nanohybrid membranes and membrane and siloxane network morphology by attuning the reaction kinetics of the sol−gel process. The CO_2 permeability of these nanohybrid membranes can reach 1810 barrer, an improvement of 7.5 folds; while H_2 permeability increase by 5.7 fold, from 30 to 170 barrer. The mechanism behind gas transport enhancements observed in these nanohybrid membranes is elucidated using positron annihilation lifetime spectroscopy and sorption measurements. Relative fractional free volume (FFV) content and CO_2 sorption behaviors in these membranes are augmented as a function of inorganic phase morphology. The CO_2 sorption behavior of the inorganic phase is regulated by the organic/inorganic ratio and water/silicon ratio in the sol−gel synthesis process. Harnessing the advantages of a unique combination of organic and inorganic materials, these nanohybrid membranes outperform most other CO_2-philic polymeric membranes.

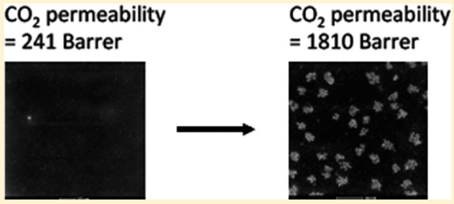

INTRODUCTION

Hydrogen (H_2), an important raw material, is commonly produced using steam hydrocarbon reforming (eq 1) while a subsequent water-gas shift reaction increases H_2 content (eq 2).[1]

$$C_nH_m + nH_2O + \text{heat} \leftrightarrow nCO + \left(\frac{m}{2} + n\right)H_2 \qquad (1)$$

$$CO + H_2O \leftrightarrow CO_2 + H_2 \qquad (2)$$

To effectively use H_2 as combustion or transportation fuel, the byproduct of carbon dioxide (CO_2) must be separated from the desired H_2 gas. Traditionally, CO_2 is separated from H_2 using high carbon footprint technologies like pressure swing adsorption and amine absorption. To reduce the footprint of these gas separation processes, a green approach like membrane technology must be advocated. The main merits of membrane technology over traditional gas separation methods are ease of application, compaction and portability, lack of moving parts, and most importantly, low footprint.[2] Prior to widespread applications of membrane technology, the inadequate gas transportation properties of dense polymeric membranes must be significantly improved.

The gas flux through a dense polymeric membrane of a known thickness characterizes gas permeability i.e. the intrinsic gas transport properties of the membrane:[3]

$$P_A = \frac{N_A l}{f_2 - f_1} \qquad (3)$$

N_A is the steady state flux through the membrane film, l is the film thickness, and f_2 and f_1 are the upstream and downstream fugacities of the gas penetrant, respectively.

The solution-diffusion mechanism describes gas permeation through dense polymeric membrane films. Assuming that the Fick's law of gas diffusion is prevalent and $f_2 \gg f_1$, permeability can be expressed as a product of solubility and diffusivity coefficients:[4]

$$P_A = S_A \times D_A \qquad (4)$$

P_A refers to the polymer permeability to gas A, while S_A is the solubility coefficient (defined as ratio of the concentration of gas A dissolved in the polymer to the fugacity of gas A in the feed side of the membrane, i.e., the upstream), and D_A refers to the average effective gas diffusion coefficient through the membrane film.

Gas separation capability i.e. gas selectivity of a membrane film is the ratio of ideal gas permeability of gas A over gas B:[3]

$$\alpha_{A/B} = \frac{P_A}{P_B} = \frac{S_A}{S_B} \times \frac{D_A}{D_B} \qquad (5)$$

D_A/D_B is the diffusivity selectivity determined primarily by the size difference between gas penetrant molecules and the size-sieving capability of the polymer matrix. S_A/S_B is the solubility selectivity that is defined mainly by the relative condensability of gas penetrants and the relative affinity of gas penetrants for the polymer matrix.

Free volume is commonly used to correlate polymer structure and gas transport properties. The Fujita-modified Cohen−

Received: May 11, 2011
Revised: June 22, 2011
Published: July 05, 2011

ACS Publications © 2011 American Chemical Society

dx.doi.org/10.1021/ma201083m | *Macromolecules* 2011, 44, 6057–6066

Turnbull free volume model can be used to describe the relationship between free volume and gas diffusivity in polymeric membranes:[5]

$$D_A = A_D \, exp\left(-\frac{B}{FFV}\right) \qquad (6)$$

A_D and B are the characteristic factors pertaining to a selected polymer−penetrant system, and FFV is the fractional free volume in the polymer. FFV characterizes chain packing efficiency and free space content that is available for gas permeation in the polymer matrix and can be determined using positron annihilation lifetime spectroscopy (PALS).[6]

The inherent gas transport and separation capabilities of polymeric membranes can be tailored via material designing.[7−11] Chen et al. designed block copolymers consisting of polyimides and poly(ethylene oxide) (PEO).[12] This combination harnesses the advantages of both materials; mechanical strength of polyimides and high CO_2 affinity of PEO resulting from a dipole−quadrupole interaction between acidic CO_2 and polar ether oxygen (EO) units. The gas transport and separation capabilities of Chen's block copolymers depend on the interaction between the PEO and polyimide content. The CO_2/H_2 separation performances of these block copolymer membranes are comparable to other innovative PEO-based block copolymer membranes.[9,11] Patel et al. cross-linked a series of low molecular weight polyether-acrylate monomers to form CO_2-philic gas separation membranes.[13] The CO_2 permeability of Patel et al.'s membranes reached 83 barrer with a CO_2/H_2 selectivity of 11. Meanwhile, Lin et al. reported the cross-linking of low M_w PEO-methyl ethyl acrylates that formed a rubbery membrane material with a CO_2 permeability of ~550 barrer and a CO_2/H_2 selectivity of 10.[14] The methyl ethyl moiety enhanced the FFV content in Lin et al.'s rubbery membranes, thus increasing CO_2 permeability when compared to Patel et al.'s membranes.

Membrane gas permeability can be enhanced via increments in diffusivity and solubility coefficients. An approach to augment diffusivity coefficients is to enhance relative FFV content via the fabrication of nanocomposite membrane materials. Nanocomposite membranes can be fabricated by the incorporation of nanoparticles into an organic polymer matrix. Merkel et al. and Patel et al. incorporated fumed silica nanoparticles into poly(4-methyl-2-pentyne) (PMP)[15] and cross-linked diacrylate-terminated poly(ethylene glycol) (PEG),[16] respectively. Positron annihilation lifetime spectroscopy (PALS) and pulse field gradient NMR data in Merkel's work show that the inclusion of silica nanoparticles improves the interconnectivity between larger concentrations of large free-volume elements. A theoretical model proposed by Hill quantitatively correlates the reverse-selectivity observed in Merkel's work to the gas permeability of polymeric nanocomposites, nanoparticle size, and free volume content.[17] In Patel et al.'s work, free volume content increments are attributed to extra free volume content at the polymer−nanoparticle interface[17] and pore size increments in the inorganic nanoparticles.[18] Nanoparticles also enhance the mechanical properties of membranes and suppress polymer crystallinity. The CO_2 transportation and separation capability of Merkel et al. and Patel et al.'s membranes and the validity of Hill's theory rely on the uniform dispersion of nanoparticles in the polymeric matrix; i.e., nanoparticle agglomeration is detrimental for gas permeability and separation. Nanoparticle agglomeration can be overcome via an *in situ* fabrication of organic−inorganic materials that yields a uniform inorganic phase in the polymeric matrix.

Using an acid-catalyzed sol−gel process, Sforça et al. synthesized an organic−inorganic material consisting of covalently bonded organic polyether diamines and inorganic epoxysilanes.[19] The CO_2/N_2 and CO_2/H_2 selectivity of this inorganic membrane are 89 and 9, respectively. Based on Sforça's approach, Shao and Chung varied the organic−inorganic ratio and reported that organic−inorganic materials consisting of 90 wt % polyether diamines possess the highest CO_2 permeability of 370 barrer with a CO_2/H_2 selectivity of 9 at 35 °C and 3.5 atm.[20] The primary aims of the inorganic phase are to impart mechanical stability and suppress crystallinity in these membranes. Improving on the work of Shao and Chung, we grafted polyether side chains onto the basic organic−inorganic material and reported that the CO_2 permeability of the modified organic−inorganic material increased to 1990 barrer.[21] The similarities in the CO_2 sorption isotherms of these modified organic−inorganic membranes and PDMS, indicate that the inorganic phase play a significant role in enhancing CO_2 permeability.[21] Additionally, the polyether grafts also increased the relative FFV content of the organic−inorganic material that leads to increments in CO_2 diffusivity. Although we have shown that the inorganic phase contributes to the CO_2 permeability of the resultant organic−inorganic material, the relationship between inorganic phase morphology and structure and CO_2 permeation is still unknown.

In this work, we attune the organic−inorganic ratio, the water/silicon ratio, and the polyether graft type to elucidate the relationship between inorganic phase morphology and CO_2 permeation. The organic/inorganic ratio was varied by adjusting the amount of organic and inorganic materials used in material synthesis while the water/silicon ratio was adjusted by varying the amount of low M_w polyether chains added during grafting. The enhancements in CO_2 permeability of the nanohybrid membranes studied in this work are dependent on inorganic phase morphology. To our best of knowledge, this is the first work that investigates the relationship between the inorganic phase morphology and the CO_2 permeation properties of nanohybrid membranes synthesized from an *in situ* approach. The findings of this work facilitate better understanding of organic−inorganic membrane material design.

■ EXPERIMENTAL SECTION

Materials. The polyether diamine used here in this work is commercially known as Jeffamine ED-2003—a poly(propylene oxide)−poly(ethylene oxide)−poly(propylene oxide) (PPO−PEO−PPO) diamine (M_w = 2000 g/mol). Poly ethylene glycol methacrylate (PEGMA: M_w = 360 g/mol), and butyl methacrylate (BuMA: M_w = 142 g/mol), ethanol (HPLC grade) and 3-glycidyloxypropyltrimethoxysilane (GOTMS: M_w = 236 g/mol) were purchased from Sigma-Aldrich, Singapore. Hydrochloric acid (HCl) was purchased from Fisher Scientific. All chemicals and solvents, except for PEGMA, were used as received. The inhibitors in PEGMA were removed using activated carbon. For every 100 mL of PEGMA, 4 g of activated carbon was added and stirred for 1 h, after which, the activated carbon was filtered from this mixture. These procedures were repeated 3 times. The purified PEGMA was stored at 4 °C.

Synthesis and Modification of Organic−Inorganic Material. A catalyzing aqueous solution containing 37.5 wt % HCl was used to hydrolyze GOTMS. After 30 min of hydrolysis at room temperature, the alkoxysilane solution was immediately added to a solution consisting 2 wt % PPO−PEO−PPO diamine dissolved in 70 wt % ethanol and

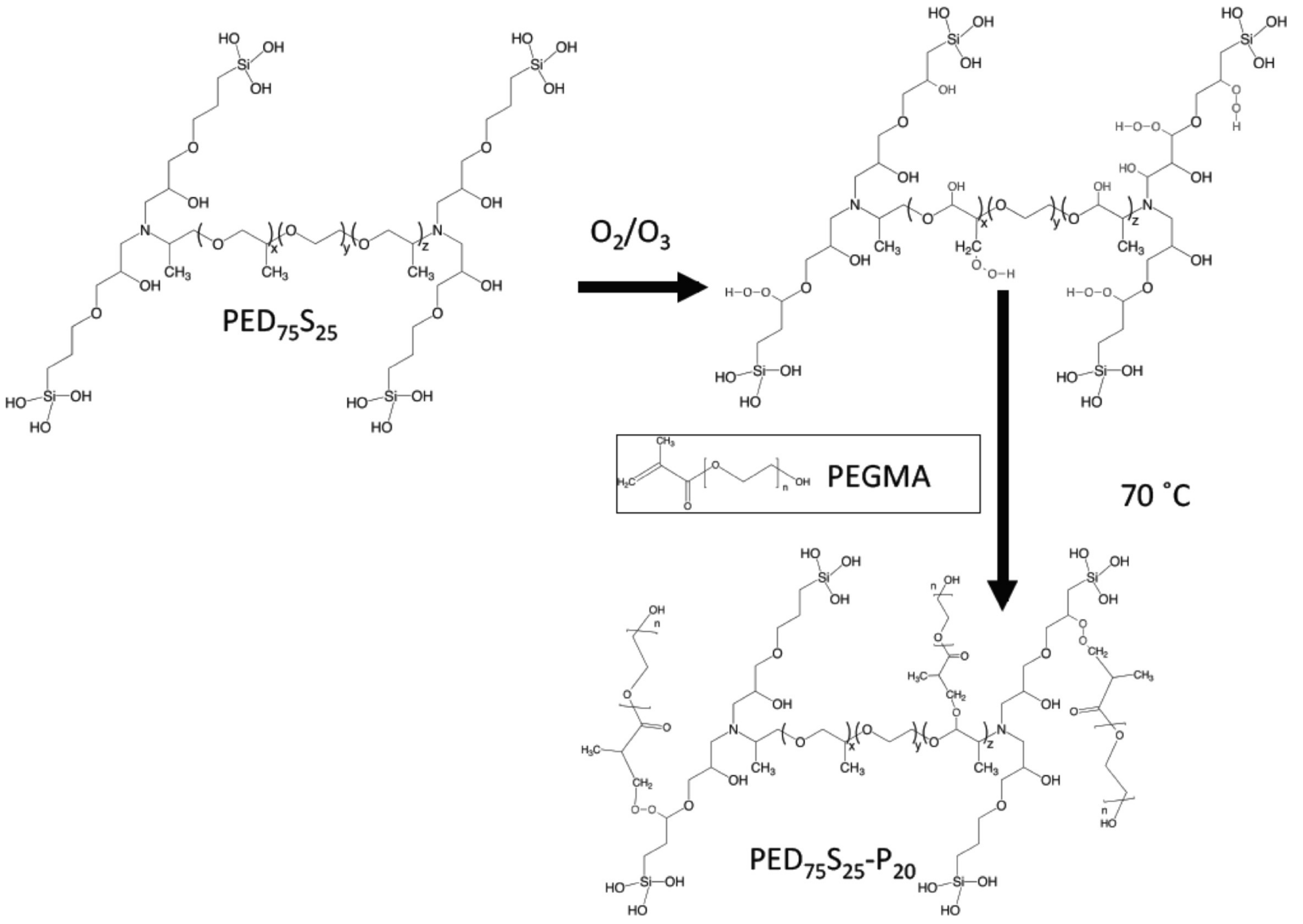

Figure 1. PEGMA is grafted onto PED$_{75}$S$_{25}$−P$_{20}$ main chains. The grafting process is initiated by the thermally decomposed peroxide moieties that are first introduced by wet ozone pretreatment.

30 wt % distilled water. The ideal molar ratio of the organic−inorganic material is 1:4 whereby each polyether diamine molecule reacts with four molecules of alkoxysilanes i.e. the ideal wt % ratio is 68 wt % of polyether to 32 wt % of alkoxysilanes. An epoxy-amine reaction was facilitated by stirring the resultant mixture at 750 rpm at 60 °C for 1 h. This organic−inorganic material is known as PED$_{XX}$S$_{XX}$ in this work whereby PED represents the polyether diamine; S denotes the alkoxysilanes while *XX* refers to the wt % of the polyether diamine and alkoxysilanes. The working organic−inorganic materials used in this study are PED$_{50}$S$_{50}$ and PED$_{75}$S$_{25}$. The solution consisting of the PEDS material was allowed to cool down to room temperature prior to 60 s of ozone pretreatment. Ozone pretreatment was carried out using an AC Faradayozone high concentration ozone generator (L10G). Then 10 psi of high purity oxygen obtained from SOXAL, Singapore, was converted into ozone (ozone flow was limited to 0.5 L per minute). Upon ozone pretreatment, short alkyl chains were added to the ozonolyzed mixture and the resultant solution was stirred at 70 °C for 24 h to facilitate alkyl side-chain grafting onto the PEDS main chains. 0−20 wt % of PEGMA (M_w 360 g/mol) was grafted onto the PED$_{50}$S$_{50}$ and PED$_{75}$S$_{25}$ materials. To determine the effects of side-chain functionality on CO$_2$ permeability, 20 wt % of BuMA was also grafted onto PED$_{50}$S$_{50}$ and PED$_{75}$S$_{25}$ materials. The organic−inorganic materials with PEGMA and BuMA grafts are known as PED$_{XX}$S$_{XX}$−P$_{YY}$, and PED$_{XX}$S$_{XX}$−B$_{YY}$, respectively. *YY* refers to the wt % of grafts. The graft concentrations were determined by comparing the weight of the membranes before and after washing. The difference in weight measurements infer to unreacted PEGMA present in the membranes.

Preparation of Organic−Inorganic Membranes. Organic−inorganic membranes were fabricated using a slow casting method. After transferring the solution into a Teflon dish, the solvent was evaporated at 30 °C for 24 h. Subsequently, the temperature was raised to 40 °C for further evaporation. Nascent films were peeled off and dried at 70 °C for 24 h to remove residual solvent while undergoing full water removal. Prior to characterization, all membranes were immersed in deionized water for 5 days to remove unreacted monomers. The deionized water was changed everyday. These nanohybrid membranes were stored in a drybox with 27% humidity at 25 °C prior to testing and characterization.

Characterization. The chemical structures of the PEDS-based nanohybrid membranes were characterized using solid-state ^{29}Si and ^{13}C NMR. The ^{29}Si (79.5 MHz) and ^{13}C (100.6 MHz) NMR with magic angle spinning (MAS) at 7.5 kHz was performed with a Bruker DRX 400 spectrometer. Samples were ground using a freeze miller prior to analysis. A Quantachrome ultrapycnometer 1200e was used to determine the density of the nanohybrid membranes studied in this work. For each sample, an average of 15 measurements with standard deviations of up to ±0.005 g/cm^3 were taken. The density measurements obtained using the pycnometer was used to calculate the solubility coefficients of the nanohybrid membranes. To determine the crystallinity, glass transition (T_g) and melting (T_m) temperatures of the nanohybrid membranes, differential scanning calorimetry (DSC) was performed using a DSC822^e (Mettler Toledo) calorimeter. The temperature range was from −100 to 100 °C with a heating rate of 10 °C/minute in a N$_2$ environment. The second heating curve was used for analysis in this work.

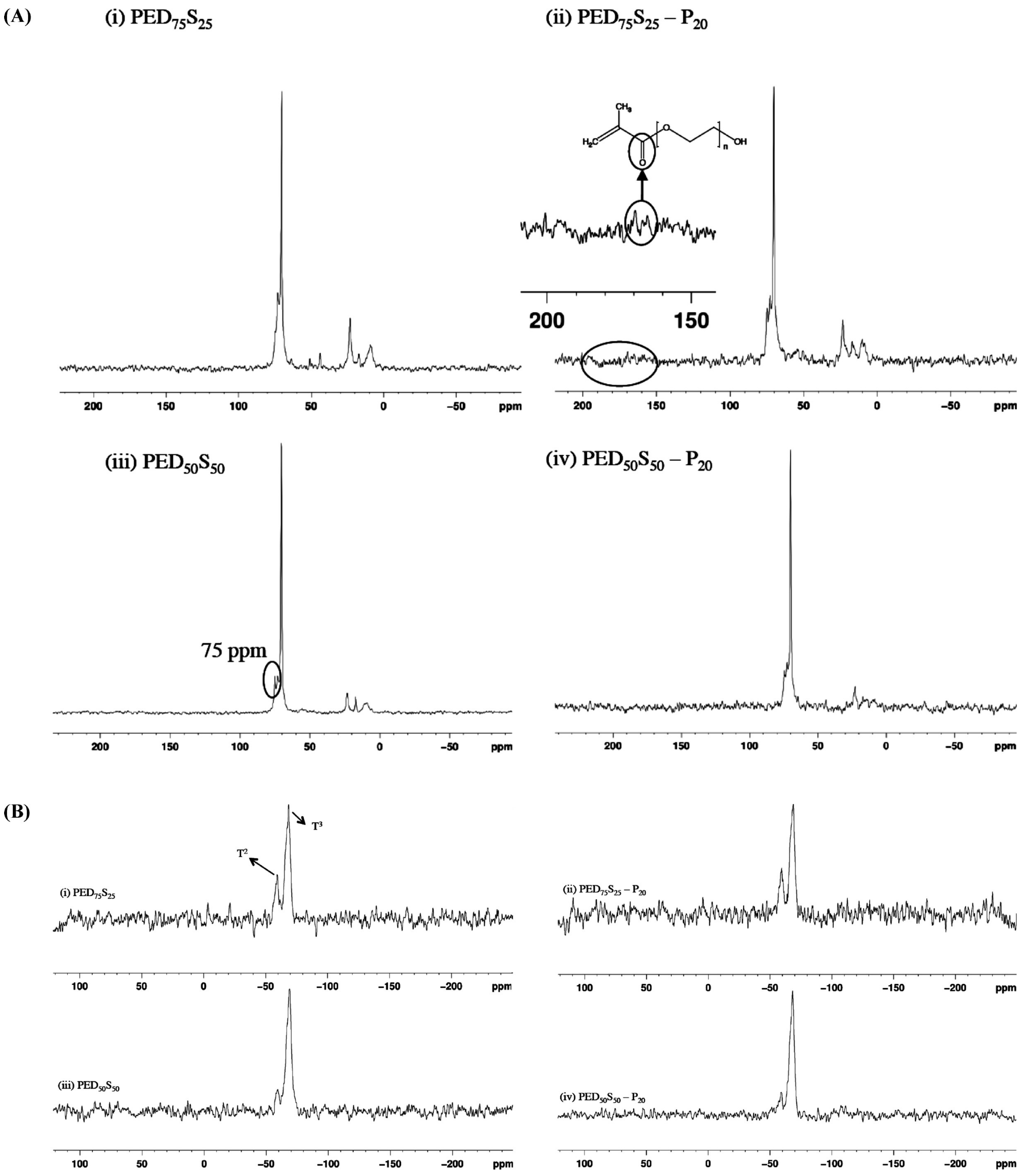

Figure 2. (A) ^{13}C NMR solid state NMR spectra of (i) $PED_{75}S_{25}$, (ii) $PED_{75}S_{25}-P_{20}$, (iii) $PED_{50}S_{50}$, and (iv) $PED_{50}S_{50}-P_{20}$ membranes. (B) ^{29}Si solid state NMR spectra of (i) $PED_{75}S_{25}$, (ii) $PED_{75}S_{25}-P_{20}$, (iii) $PED_{50}S_{50}$, and (iv) $PED_{50}S_{50}-P_{20}$ membranes.

Scanning Transmission Electron Microscopy (STEM). STEM was used to observe the inorganic phase morphology and dispersion. To prepare samples for STEM characterization, solutions containing nanohybrid materials were diluted from 2 wt % to 0.01 wt %. The high-angle annular dark field scanning—TEM (HAADF—STEM) studies and EDX analysis were carried out on a FEI Titan 80—300 electron microscope that was equipped with an electron beam monochromator, an energy dispersive X-ray spectroscopy (EDX) and a Gatan electron energy loss spectrometer. The accelerating voltage of the electron beam was 200 KeV. The scanning electron beam size of EDX measurement was around 0.3 nm.

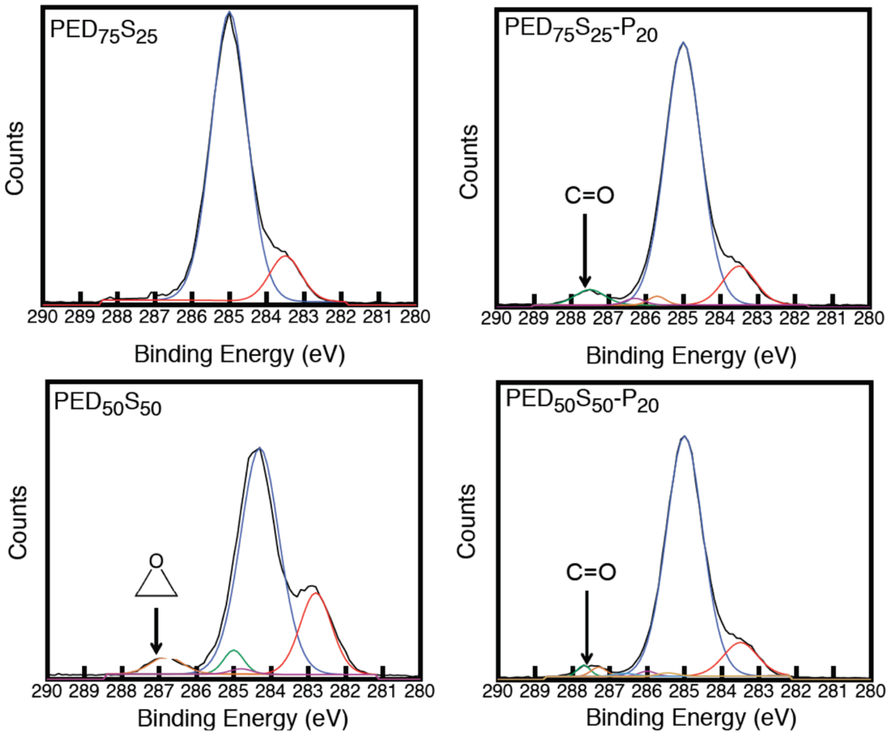

Figure 3. XPS spectra of PEDS membranes.

Positron Annihilation Spectroscopy. To prepare the nanohybrid samples for positron annihilation lifetime (PAL) characterization, a positron source (50 mCi ^{22}Na purchased from iThemba Laboratories, South Africa) was sandwiched in between two pieces of the membrane samples (1 cm ×1 cm) that was sealed in between two 12 μm thick Kapton films. The assembled samples were exposed to different temperatures and CO_2 pressures in a specially designed setup that was described previously.[6] CO_2 pressure in this setup was monitored using an Omega transducer pressure gauge (Model 302−1KGY). The positron annihilation lifetime (PAL) spectra were recorded using a fast−fast coincident PAL spectrometer (resolution = 280 ps) at the University of Missouri—Kansas City. The acquired PAL spectra (1 million counts) were analyzed into 3-mean lifetimes and into lifetime distributions using PATFIT and MELT computer programs. The longest lifetime from these analyses (τ_3 in ns) is due to the pick off annihilation of orthopositroniums (*o*-Ps) in free volume cavities (V_f). The V_f mean radius and volume were tabulated using well-established semiempirical equations based on the spherical infinite potential-well model.[22,23] The V_f radii size distribution correlates to τ_3 (in ns) of *o*-Ps while *o*-Ps intensity (I_3 in %) correlates to *o*-Ps formation, i.e., V_f content.[6] Using the I_3 and τ_3 values, the relative free fractional volume (FFV) of these nanohybrid materials are estimated by assuming that free volume is spherical and the equation, $AV_f I_3$, whereby A is an empirical constant and $V_f = 4\pi R^3/3$.[6]

Gas Permeability Measurements. The pure gas permeabilities were determined using a constant volume and variable pressure method. Detailed experimental design and procedures have been reported elsewhere.[24] The gas permeabilities of H_2 and CO_2 at 3.5 atm were determined from the rate of downstream pressure build-up rate (dp/dt) obtained when permeation reached a steady state according to eq 9:

$$P = D \times S = \frac{273 \times 10^{10}}{760} \frac{VL}{AT\left[\frac{p_2 \times 76}{14.7}\right]}\left(\frac{dp}{dt}\right) \qquad (9)$$

where P is the permeability of a membrane to a gas and its unit is in Barrer (1 barrer =1 × 10^{-10} cm^3 (STP)-cm/cm^2 s cmHg), D is the average effective diffusivity (cm^2/s), S is the apparent sorption coefficient/solubility (cm^3 (STP)/cm^3 polymer cmHg), V is the volume of the downstream chamber (cm^3), and L is the film thickness (cm). A refers to the effective area of the membrane (cm^2), T is the experimental temperature (K), and the pressure of the feed gas in the upstream chamber is given by p_2 (psia).

CO_2 Sorption Measurements. Carbon dioxide sorption tests were conducted using a Cahn D200 microbalance sorption cell at 35 °C over a pressure range of 0−250 psi (0−17.24 bar). A detailed description of the dual volume sorption cell was reported elsewhere.[24] For each sample, films with thickness of 300 μm, sides of 1 cm, and total mass of approximately 80−100 mg were placed on the sample pan. The system was evacuated for 24 h prior to testing. The gas at a specific pressure was fed into the system. The mass of gas sorbed by the membranes at equilibrium was recorded. Subsequent sorption experiments were done by further increment of the gas pressure. The buoyancy force corrected the equilibrium sorption value obtained. CO_2 solubility coefficients of each sample were obtained from the gradient of the sorption isotherms. Subsequently, CO_2 diffusivity coefficients were calculated using eq 4.

■ RESULTS AND DISCUSSION

Characterization of Organic−Inorganic Material Structure. Following our previous approach,[21] an organic−inorganic material comprising a low molecular weight poly(propylene oxide) (PPO)−PEO−PPO diamine and 3-glycidyloxypropyltrimethoxysilane (GOTMS), an alkoxysilane, is first synthesized using an acid catalyzed sol−gel reaction. To facilitate polyether grafting on the PEDS organic−inorganic material, peroxide moieties that serve as initiation sites must first be introduced on to the main chains of the PEDS material. Following the approach adopted by Chen et al., the CH_x sites in the organic−inorganic materials are first converted into peroxide moieties using a wet ozone pretreatment.[25] Subsequent thermal decomposition of these peroxide moieties provide initiation sites for the grafting of short polyether chains onto the main PEDS material. Figure 1 shows the synthesis route and chemical structures of the PEDS nanohybrid membranes.

The nonideal molar ratio between the organic polyether diamines and the inorganic alkoxysilanes in a PED$_{75}$S$_{25}$ membrane results in excess polyether diamines. Hence, in the ^{13}C NMR spectrum of a PED$_{75}$S$_{25}$ membrane (Figure 2), the peak at δ = 43.9 ppm correlates to C−N bonds found in $-\mathrm{CH_2NH_2}$ moieties.[26] In the case of a PED$_{50}$S$_{50}$ membrane, the nonideal molar ratio yields excess inorganic alkoxysilanes. Thus, in the ^{13}C NMR spectrum of a PED$_{50}$S$_{50}$ membrane, the peak corresponding to a C−Si bond at δ = 79 ppm is more obvious in the ^{13}C NMR spectrum of a PED$_{50}$S$_{50}$ membrane, indicating the presence of excess alkoxysilanes. In the ^{13}C NMR spectrum of a PED$_{75}$S$_{25}$−P$_{20}$ membrane, a peak at δ = 170 ppm corresponds to a C═O terminal group[26] validate the presence of PEGMA grafts on the PEDS main chains. Peaks corresponding to C═C (between δ = 115 - 140 ppm) are absent in the PEGMA-grafted nanohybrid membranes i.e. unreacted PEGMA is successfully removed from the nanohybrid membranes after washing. The T^2 and T^3 resonance peaks (δ = −59 ppm and −67 ppm) in the ^{29} Si solid-state NMR spectra indicate that the inorganic networks in the PEDS-based organic−inorganic materials consist a mixture of silicons that consist of two siloxane and one ethoxy or hydroxyl bonds (T^2) or are fully condensed with three siloxane bonds (T^3).[19,27]

The C 1s peak at approximately 287 eV corresponds to the carbon atoms in an epoxy ring.[28] This peak is prominent only in the X-ray photoelectron spectroscopy (XPS) spectra of PED$_{50}$S$_{50}$ membranes (Figure 3); validating the presence of excessive epoxysilanes. The excessive epoxysilanes are completely hydrolyzed and condensed into silicons with two or three siloxane bonds. This is evidenced by the absence of T^0, and T^1 peaks in the solid-state ^{29}Si NMR spectra. In the case of PED$_{75}$S$_{25}$ membranes, all epoxysilanes reacted with polyether diamines hence the C 1s peak that belongs to the C 1s atom of an epoxy ring at 287 eV is not obvious. The peaks between 287−288 eV in the XPS spectra of PED$_{50}$S$_{50}$−P$_{20}$ and PED$_{75}$S$_{25}$−P$_{20}$ membranes indicate the presence of C═O moieties (present in PEGMA). As these PED$_{50}$S$_{50}$−P$_{20}$ and PED$_{75}$S$_{25}$−P$_{20}$ membranes are characterized after the removal of unreacted PEGMA, the presence of C═O moieties result from the PEGMA grafts in the materials.

Morphology of PEDS and PEDS−P$_{xx}$ Organic−Inorganic Materials. Organic−inorganic materials can be synthesized using an acid-catalyzed sol−gel process[19,20,29] whereby inorganic morphology and dispersion are controlled by the reaction kinetics of the sol−gel process. The sol−gel process involves two reactions involving the silicon atom as follows:[29]

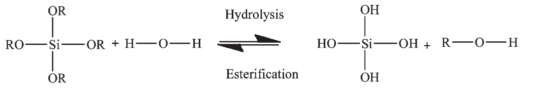

$$\mathrm{RO{-}Si(OR)_2{-}OR + H{-}O{-}H \underset{\text{Esterification}}{\overset{\text{Hydrolysis}}{\rightleftharpoons}} HO{-}Si(OH)_2{-}OH + R{-}O{-}H} \qquad (7)$$

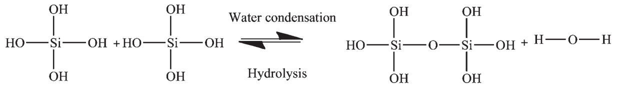

$$\mathrm{HO{-}Si(OH)_2{-}OH + HO{-}Si(OH)_2{-}OH \underset{\text{Hydrolysis}}{\overset{\text{Water condensation}}{\rightleftharpoons}} HO{-}Si(OH)_2{-}O{-}Si(OH)_2{-}OH + H{-}O{-}H} \qquad (8)$$

Hydrolysis occurs over a nucleophilic attack by the oxygen in water on the silicon atom. As an acid-catalyzed hydrolysis promotes the protonation of alkoxides in alkoxysilanes, the electron density withdrawal of the silicon atom makes it more electrophilic and more susceptible to an attack by water. With increased electrophilicity, the water molecule attacks and imparts a positive partial charge to the protonated alkoxides.[30] A subsequent reduction of this partial charge facilitates an alcohol departure from the silicon tetrahedron. Water condensation removes water from the system and minimizes depolymerization, thus resulting in an insoluble three-dimensional siloxane network. When depolymerization is least likely to reoccur, condensation becomes irreversible and the hydrolysis of siloxane bonds after formation is impossible. Condensation involves a nucleophilic attack on the deprotonated silanol in a neutral silicate species and is essential for the siloxane network development.[31] The siloxane network formation is a sequential product of hydrolysis, condensation, and the reverse reactions and is therefore dependent on the H$_2$O/Si ratio,[29] the organic/inorganic ratio, and the glass transition temperature (T_g) of the organic phase.[32]

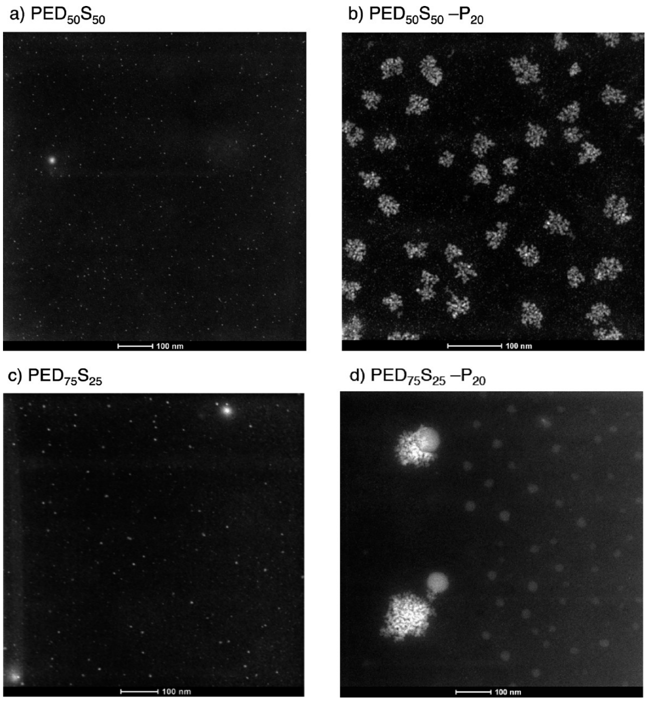
a) PED$_{50}$S$_{50}$ b) PED$_{50}$S$_{50}$ −P$_{20}$ c) PED$_{75}$S$_{25}$ d) PED$_{75}$S$_{25}$ −P$_{20}$

Figure 4. STEM images of PEDS nanohybrid membranes.

Effect of Water/Silicon (H$_2$O/Si) and Organic−Inorganic Ratio on the Morphology of Organic−Inorganic Materials. STEM images in Figure 4 indicate that the inorganic phase exists as nanostructures in the organic−inorganic materials. Energy dispersive X-ray spectroscopy has shown that these inorganic nanostructures are primarily made up of silicon and oxygen. With reference to Figure 2B, the silicon atoms in these nanohybrid materials are fully condensed and bond to three siloxane (Si−O−Si) bonds or partially condensed with two siloxane bonds and an ethoxy or methoxy moiety. Hence, we can assume that these nanoparticle-lookalike structures are the agglomerations of a siloxane network. The acid-catalyzed, two step sol−gel process used in this work leads to the formation of siloxane networks in a polyether matrix. In the initial hydrolysis step of our approach, complete hydrolysis ensued as the H$_2$O/Si ratio <4, i.e., hydrolysis and condensation are rate limiting and depolymerization rates are low.[29] The relatively low depolymerization rate results in rate limiting cluster−cluster aggregation that forms weakly branched, rough-edged siloxane networks.[33] In

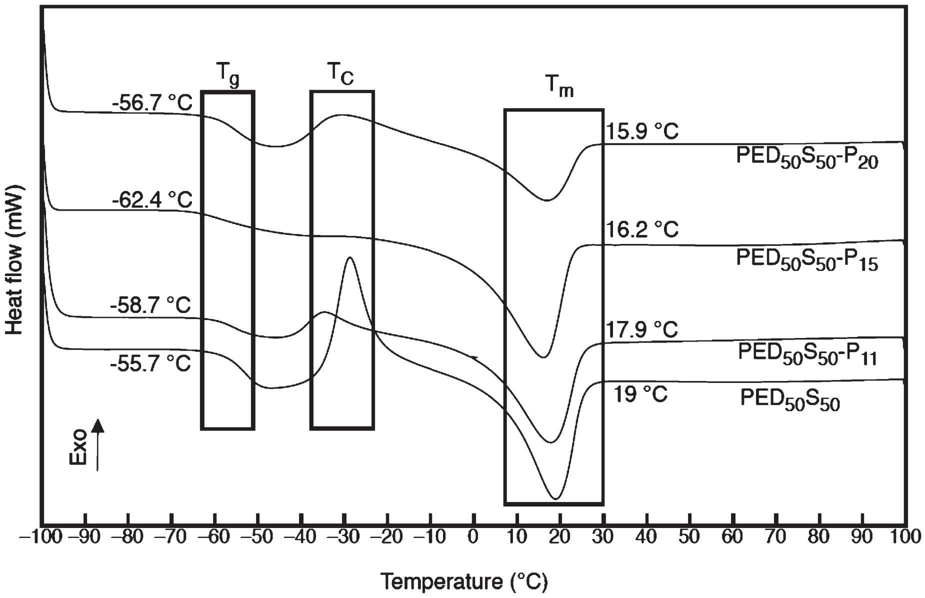

Figure 5. DSC spectra of $PED_{50}S_{50}$, $PED_{50}S_{50}-P_{11}$, $PED_{50}S_{50}-P_{15}$, and $PED_{50}S_{50}-P_{20}$ nanohybrid membranes.

the second synthesis step, the hydrolysis solution is mixed with a solution of polyether diamine dissolved in ethanol/water (70 wt %/30 wt %) i.e. H_2O/Si ratio $\gg$4. With a large H_2O/Si ratio, condensation and reconstruction proceeds concurrently at comparable rates. The siloxane network growth process becomes similar to a nucleation and growth process i.e. a monomer-cluster aggregation and results in smooth looking siloxane networks when water is absent from the system.[29] Smooth-looking siloxane networks are observed in $PED_{50}S_{50}$ and $PED_{75}S_{25}$ nanohybrid membranes. Unreacted short alkyl chains, e.g., PEGMA can also decrease the H_2O/Si ratio and increase hydrolysis rates during depolymerization. As PEG forms hydrogen bonds with water easily, the reduction in the concentration of "free" water molecules that engage in siloxane network development lowers the H_2O/Si ratio. With lower a H_2O/Si ratio, the siloxane network evolve from a smooth-looking nanostructure (in PEDS nanohybrid membranes) to rough clusters (in PEGMA-grafted PEDS nanohybrid membranes).[29] The siloxane network growth at a low H_2O/Si ratio is governed by the cluster−cluster aggregation mechanism. Additionally, the presence of unreacted PEGMA also increases the organic/inorganic ratio.

Siloxane network sizes increase as a function of increasing polyether content, i.e., when organic−inorganic ratio increases by the incorporation of more polyether diamines or by grafting short alkyl chains. In $PED_{50}S_{50}$ nanohybrid membranes, the average siloxane agglomeration size is 5 nm while in $PED_{75}S_{25}$ nanohybrid membranes; the average siloxane agglomeration size is 7 nm. When PEGMA is grafted onto the PEDS main chains, siloxane agglomerations become larger and more obvious. With 20 wt % PEGMA grafts, siloxane agglomerations increase from ~5 to 140 nm in $PED_{50}S_{50}-P_{20}$ membranes, while siloxane agglomerations increase from ~7 to 190 nm in $PED_{75}S_{25}-P_{20}$ membranes. In this work, the increase in organic/inorganic ratio is facilitated with the engagement of more polyethers during synthesis and reducing epoxysilane content. This dilution effect affects siloxane network dispersion in the polymer matrix. In the $PED_{75}S_{25}$ series, all the diamines and epoxy undergo the epoxy-diamine reaction in the presence of excess diamines. Consequently, the excess diamines result in a reduced water/silicon ratio and promote reaction-limited cluster−cluster agglomeration, thus forming bigger siloxane agglomerations.

Effects of Ostwald Ripening and Organic Phase T_g. Ostwald ripening is the effect of nanostructure agglomeration in which small nanostructures form a few large clusters with lower surface energy that is thermodynamically favored and is prevalent when depolymerization takes place.[27] As depolymerization is widespread in the process of water removal, nanostructure agglomeration in these organic−inorganic materials is common, hence siloxane network agglomeration is also a contributing factor that leads to the larger siloxane networks observed in Figure 4, parts c and d. Another factor that may contribute to siloxane network agglomeration is the vitrification of the sol−gel reaction. Sol−gel vitrification is dependent on the glass-transition temperature (T_g) of the organic phase that governs the morphology growth mechanism in organic−inorganic materials. Lower T_gs attribute to a larger condensation extent that consequently leads to bigger siloxane networks.[32] From Figure 5, it is evident that PEGMA grafts reduce the T_g of these nanohybrid membranes. STEM images in Figure 4 show that the siloxane networks in $PED_{50}S_{50}-P_{20}$ membranes are bigger in size when compared to those observed in $PED_{50}S_{50}$ membranes. The combination of lower H_2O/Si ratios, higher organic−inorganic ratios, and Ostwald ripening leads to the agglomeration of siloxane networks that may also affect the relative fractional free volume content in the membrane material.

Relative Fractional Free Volume Content in Nanohybrid Membranes. Figure 6a shows that the relative FFV content determined using PALS in $PED_{50}S_{50}$ materials is lower when compared to $PED_{75}S_{25}$ materials. In $PED_{50}S_{50}$ membranes, excess alkoxysilanes may result in some mobile siloxane networks that are not immobilized by the $PED_{50}S_{50}$ main chains. Hence, when siloxane network agglomeration takes place in $PED_{50}S_{50}$ materials, main chain contortion will be less severe when compared to siloxane network agglomeration in $PED_{75}S_{25}$ materials whereby most siloxane networks are immobilized. In $PED_{75}S_{25}$ membranes, all alkoxysilanes are involved in the

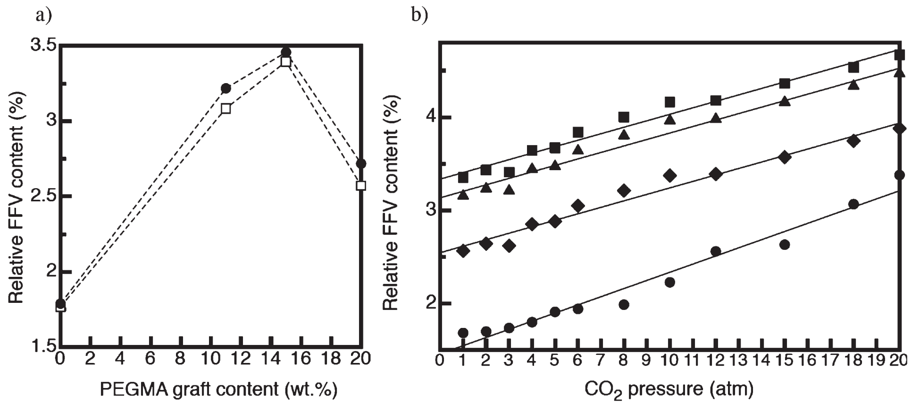

Figure 6. (a) Relative FFV content of $PED_{75}S_{25}$ (solid circle) and $PED_{50}S_{50}$ (empty square) nanohybrid membranes as a function of PEGMA graft content (wt %). (b) Relative FFV content of $PED_{75}S_{25}$ (circle), $PED_{75}S_{25}-P_{11}$ (triangle), $PED_{75}S_{25}-P_{15}$ (square), and $PED_{75}S_{25}-P_{20}$ (diamond) as a function of CO_2 pressure.

epoxy-diamine reaction with polyether diamines and the silanes are immobilized in fixed positions by the polyethers. When the silanes are condensed into siloxane networks, main chain contortions in $PED_{75}S_{25}$ membranes are more pronounced when compared to those in $PED_{50}S_{50}$ membranes. Ascribing to more pronounced main chain contortions and possible steric and kinetic constraints that inhibit siloxane network interpenetration and condensation; the spaces in between siloxane networks in $PED_{75}S_{25}$ materials are not as filled up as those in $PED_{50}S_{50}$ materials i.e. higher relative FFV in $PED_{75}S_{25}$ materials. According to eq 6, a lower relative FFV content can induce lower diffusivity coefficients. Consequently, gas diffusivities and permeabilities of $PED_{50}S_{50}$ membranes are predicted to be lower when compared to $PED_{75}S_{25}$ membranes that possess a higher relative FFV content.

The linear relationships between relative FFV in both $PED_{75}S_{25}$ and $PED_{75}S_{25}-P_{20}$ nanohybrid materials and CO_2 pressure in Figure 6b indicate that Henry's law dominates CO_2 sorption below 20 atm in these nanohybrid membranes. On the basis of Henry's law, CO_2 sorption is achieved via the swelling of existing free volume or the creation of new CO_2 sorption sites.[6] Additionally, the relative FFV content increases as a function of PEGMA graft content. The relative FFV content in $PED_{75}S_{25}-P_{15}$ membranes is higher than that in $PED_{75}S_{25}-P_{20}$ membranes. With higher PEGMA graft content in $PED_{75}S_{25}-P_{20}$ membranes, the PEGMA side chains are possibly longer. Longer PEGMA side chains can form hydrogen bonds with neighboring PEDS main chains or PEGMA side chains. This inhibits chain mobility and thus reduces relative FFV content. Coupled with the morphology of the inorganic phase, the relative FFV content plays an important role in determining the gas permeation and separation properties of the organic–inorganic materials.

Gas Permeability Measurements of the Organic–Inorganic Materials. The ideal CO_2 (200 barrer) and H_2 (28 barrer) permeabilities of $PED_{50}S_{50}$ membranes are similar to membranes with the same chemical composition in Shao and Chung's work.[20] Compared to the P_{CO_2} and P_{H_2} of $PED_{50}S_{50}$ in Figure 7, P_{CO_2} and P_{H_2} of $PED_{50}S_{50}-P_{20}$ increase by 5.3 and 4.4 fold. In the $PED_{75}S_{25}-P_{20}$ nanohybrid membrane series, P_{CO_2} and P_{H_2} increase by 7.5 and 5.7 fold. The mixed gas permeabilities of $PED_{75}S_{25}-P_{xx}$ membranes are similar to ideal gas permeabilities (not shown here). The CO_2/H_2 permselectivity data is shown in Table 1. The larger increment in P_{CO_2} permeability of the PED_{75}-$S_{25}-P_{20}$ can be ascribed to higher polyether content and higher relative FFV content, while the higher relative FFV content attributes to the larger increment in P_{H_2} permeability. Nanohybrid membranes with alkyl methacrylate grafts comprising 5–10 EO units (PEGMA) display higher P_{CO_2} and P_{H_2} compared with membranes with alkyl methacrylates consisting of one EO unit (BuMA). Congruent with other works,[19–21,30] the observed larger P_{CO_2} jumps in $PED_{75}S_{25}-P_{xx}$ nanohybrid membranes correlates to higher ethylene oxide content and more importantly, morphological changes in siloxane networks.

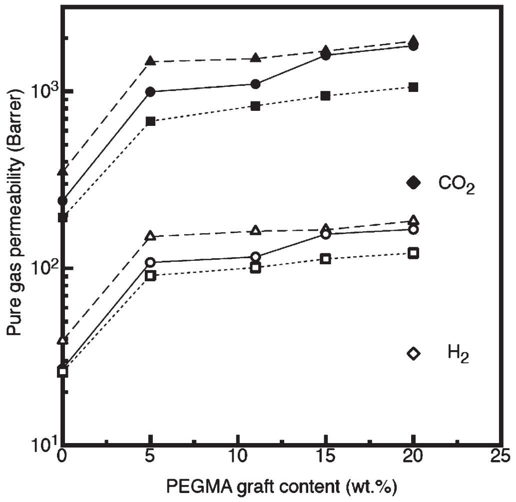

Figure 7. Pure gas permeabilities of $PED_{50}S_{50}$(sqaures), $PED_{75}S_{25}$-(circles), $PED_{80}S_{20}$(triangles)[21] nanohybrid membranes with different PEGMA graft content and $PED_{75}S_{25}$– $BuMA_{20}$(diamonds). The solid and empty symbols represent CO_2 and H_2 permeability, respectively. The lines are drawn to provide a guide to the eye. Uncertainty in gas permeabilities is around ±10%.

Compared with membranes without PEGMA grafts, the S_{CO_2} coefficients of PEGMA-grafted nanohybrid membranes are enhanced by approximately 1.4 fold. As ethylene oxide moieties preferentially interacts with CO_2 penetrants, the higher EO content in $PED_{75}S_{25}-P_{xx}$ nanohybrid membranes results in larger S_{CO_2} coefficients when compared to $PED_{50}S_{50}-P_{xx}$ nanohybrid membranes. Additionally, the morphology of the siloxane networks contributes to enhanced S_{CO_2} and P_{CO_2} coefficients.

Table 1. Gas Permeability and Permselectivity of Nanohybrid Membranes Studied in This Work

sample code	P_{CO_2} (Barrer)	P_{H_2} (Barrer)	CO_2/H_2 selectivity
$PED_{50}S_{50}-P_{00}$	193	26	7.4
$PED_{50}S_{50}-P_{05}$	678	91	7.5
$PED_{50}S_{50}-P_{11}$	829	101	8.2
$PED_{50}S_{50}-P_{15}$	943	113	8.4
$PED_{50}S_{50}-P_{20}$	1060	122	8.7
$PED_{75}S_{25}-P_{00}$	241	27	8.9
$PED_{75}S_{25}-P_{05}$	994	108	9.2
$PED_{75}S_{25}-P_{11}$	1100	116	9.5
$PED_{75}S_{25}-P_{15}$	1600	156	10.3
$PED_{75}S_{25}-P_{20}$	1810	166	10.9
$PED_{75}S_{25}-BuMA_{20}$	305	33	9.5

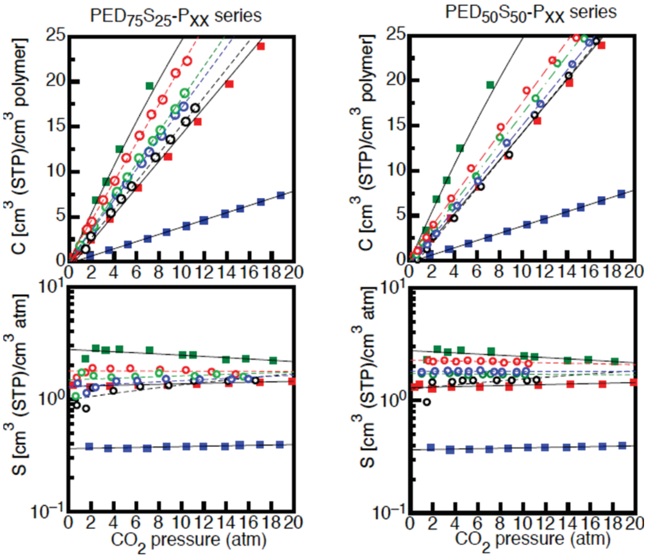

Figure 8. Sorption isotherms and solubility coefficients of PEDS nanohybrid membranes. The colored squares denote the sorption isotherms and solubility coefficients of semicrystalline PEO (blue), PDMS (pink), PTMSP (green). The empty colored circles represent nanohybrid membranes containing 0 wt % (black), 11 wt % (green), 15 wt % (blue), and 20 wt % (red) PEGMA grafts.

Ostwald ripening and changes in organic−inorganic ratio cause the agglomeration of siloxane networks (5−10 nm) into well-dispersed bigger siloxane networks (140−190 nm). As Si−O bonds possess good CO_2 affinity,[34] the siloxane networks can significantly contribute to CO_2 sorption. In Figure 8, the CO_2 sorption isotherms of $PED_{75}S_{25}-P_{xx}$ and $PED_{50}S_{50}-P_{xx}$ membranes resemble the CO_2 sorption of polydimethylsiloxane (PDMS) and the S_{CO_2}coefficients increase as a function of PEGMA-graft content (from 0 to 20 wt %). These signify that the inorganic phase is fundamental for enhanced CO_2 permeabilities in these nanohybrid membranes. Interestingly, CO_2 permeability and solubility increases as a function of siloxane network size. To date, there is no exact method to elucidate the relationship between siloxane network size and CO_2 permeability and solubility trends. The 1.4-fold increase in S_{CO_2} coefficients of $PED_{75}S_{25}-P_{xx}$ membranes is insufficient to register a 7.5-fold increase in P_{CO_2} coefficients. It is evident that increments in D_{CO_2} coefficients lead to the significant jumps observed in P_{CO_2}.

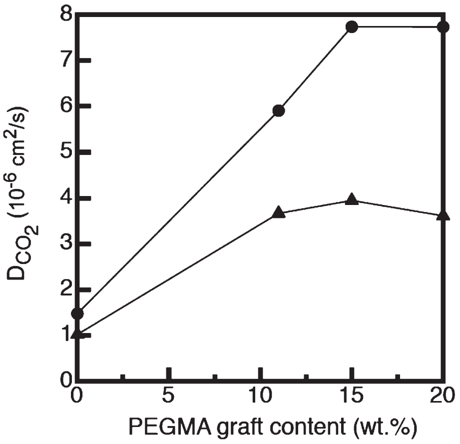

Figure 9. Diffusivity coefficients of PEDS nanohybrid membranes. Solid circles and triangles represent $PED_{75}S_{25}$ and $PED_{50}S_{50}$ nanohybrid membranes, respectively.

D_{CO_2} coefficients are determined using eq 4 i.e. $D = P/S$ and are shown in Figure 9. Similar to S_{CO_2} coefficients, D_{CO_2} coefficients increase as a function of PEGMA content (from 0 wt % to 20 wt %). *In situ* fabrication of organic−inorganic materials usually yields a morphology that is similar to a polymeric phase filling up the open pores of a silica aerogel.[28] In this work, the opposite polarity between the organic and inorganic phases prohibits complete filling up of the open pores.[35] Moreover, the agglomeration of the siloxane networks prohibits interpenetration and condensation that can fill up the space between the siloxane networks. These lead to open-porosity that consequently enhances relative FFV content across all classes of PEGMA-grafted nanohybrid membranes. In nanohybrid membranes with 20 wt % PEGMA grafts, D_{CO_2} coefficients are lower than the D_{CO_2} coefficients of nanohybrid membranes with 10 and 15 wt % PEGMA grafts. Higher PEGMA content, i.e., 20 wt % of PEGMA grafts leads to larger or longer PEGMA side chains that are more susceptible to form hydrogen bonds (via −OH moieties) with neighboring PEDS main chains or PEGMA side chains; resulting in reduced chain mobility that decreases FFV content. As diffusivity coefficients are inversely related to FFV content, enhanced relative FFV content increases diffusivity coefficients, i.e., gas transport channels for gas diffusion. D_{CO_2} coefficients increase by 5.2 times and by 3.5 times in $PED_{75}S_{25}-P_{xx}$ and $PED_{50}S_{50}-P_{xx}$ membranes, respectively. As the working materials have good CO_2 affinity, H_2 permeability increments can be ascribed to the increase in relative FFV content and diffusivity coefficients.

■ CONCLUSIONS

The incorporation of ethylene oxide-based side chains reduces the overall concentration of moieties with good CO_2 affinity in relation to those without CO_2 affinity. This highlights the influence of inorganic phase morphologies on gas permeability, in particular CO_2 permeability. The underlying reason behind the observed significant jumps in CO_2 permeability is the increase in both solubility and diffusivity coefficients. Larger siloxane networks leads to higher CO_2 solubility while significantly enhancing free volume content in the nanohybrid membranes. The CO_2 permeability values of nanohybrid membranes studied in this work are in the same magnitude as the CO_2 permeability values of PDMS, the most permeable rubbery polymer, while H_2

permeability of these nanohybrid membranes is much lower than that of PDMS. This marks an improvement in CO_2/H_2 selectivity. The remarkable CO_2 transportation capabilities of these nanohybrid membranes facilitate possible large-scale nanohybrid membrane applications.

AUTHOR INFORMATION

Corresponding Author

*E-mail: chencts@nus.edu.sg.

ACKNOWLEDGMENT

We would like to thank the Singapore National Research Foundation (NRF) for support through the Competitive Research Program for the project entitled, "Molecular engineering of membrane materials: research and technology for energy development of hydrogen, natural gas and syngas" (grant number R-279-000-261-281). We also thank Dr. Donald Paul, Dr. Liu Songlin, Dr. Xiao Youchang, Dr. Li Yi and Ms Chua Meiling and Ms Wang Huan for their assistance and valuable suggestions during this work; and Dr. Yan-Ching Jean and Dr. Hongmin Chen for their assistance in PALS experiments.

REFERENCES

(1) Hočevar, S.; Summers, W. *Hydrogen Technology*: Springer-Verlag: Berlin and Heidelberg, Germany, 2008.

(2) Shao, L.; Low, B. T.; Chung, T. S.; Greenberg, A. R. *J. Membr. Sci.* **2009**, *327*, 18–31.

(3) Koros, W. J.; Fleming, G. K. *J. Membr. Sci.* **1993**, *83*, 1–80.

(4) Wijmans, J. G.; Baker, R. W. *J. Membr. Sci.* **1995**, *107*, 1–21.

(5) Fujita, H. *Diffusion in polymer-diluent systems*; Springer-Verlag: Berlin and Heidelberg, Germany, 1961.

(6) Chen, H.; Cheng, M. L.; Jean, Y. C.; Lee, L. J.; Yang, J. *J. Polym. Sci., Part B: Polym. Phys.* **2008**, *46*, 388–405.

(7) Merkel, T. C.; He, Z.; Pinnau, I.; Freeman, B. D.; Meakin, P.; Hill, A. J. *Macromolecules* **2003**, *36*, 6844–6855.

(8) Kim, J. H.; Min, B. R.; Kim, C. K.; Won, J.; Kang, Y. S. *Macromolecules* **2001**, *34*, 6052–6055.

(9) Okamoto, K.-i.; Fuji, M.; Okamyo, S.; Suzuki, H.; Tanaka, K.; Kita, H. *Macromolecules* **1995**, *28*, 6950–6956.

(10) Yave, W.; Car, A.; Funari, S. S.; Nunes, S. P.; Peinemann, K.-V. *Macromolecules* **2009**, *43*, 326–333.

(11) Yave, W.; Car, A.; Peinemann, K.-V.; Shaikh, M. Q.; Rätzke, K.; Faupel, F. *J. Membr. Sci.* **2009**, *339*, 177–183.

(12) Chen, H. Z.; Xiao, Y.; Chung, T. S. *Polymer* **2010**, *51*, 4077–4086.

(13) Patel, N. P.; Miller, A. C.; Spontak, R. J. *Adv. Mater.* **2003**, *15*, 729–733.

(14) Lin, H.; Van Wagner, E.; Swinnea, J. S.; Freeman, B. D.; Pas, S. J.; Hill, A. J.; Kalakkunnath, S.; Kalika, D. S. *J. Membr. Sci.* **2006**, *276*, 639–642.

(15) Merkel, T. C.; Freeman, B. D.; Spontak, R. J.; He, Z.; Pinnau, I.; Meakin, P.; Hill, A. J. *Science* **2002**, *296*, 519–522.

(16) Patel, N. P.; Miller, A. C.; Spontak, R. J. *Adv. Funct. Mater.* **2004**, *14*, 699–707.

(17) Hill, R. J. *Phys. Rev. Lett.* **2006**, *96*, 216001.

(18) Voronin, E. F.; Gun'ko, V. M.; Guzenko, N. V.; Pakhlov, E. M.; Nosach, L. V.; Leboda, R.; Skubiszewska-Zieba, J.; Malysheva, M. L.; Borysenko, M. V.; Chuiko, A. A. *J. Colloid Interface Sci.* **2004**, *279*, 326–340.

(19) Sforça, M. L.; Yoshida, I. V. P.; Nunes, S. P. *J. Membr. Sci.* **1999**, *159*, 197–207.

(20) Shao, L.; Chung, T. S. *Int. J. Hydrogen Energ.* **2009**, *34*, 6492–6504.

(21) Lau, C. H.; Liu, S.; Paul, D. R.; Xia, J.; Jean, Y.-C.; Chen, H.; Shao, L.; Chung, T. S. *Adv. Energ. Mater.* **2011**.

(22) Eldrup, M.; Lightbody, D.; Sherwood, J. N. *Chem. Phys.* **1981**, *63*, 51–58.

(23) Tao, S. J. *J. Chem. Phys.* **1971**, *56*, 5499.

(24) Wang, R.; Cao, C.; Chung, T. S. *J. Membr. Sci.* **2002**, *198*, 259–271.

(25) Chen, Y.; Ying, L.; Yu, W.; Kang, E. T.; Neoh, K. G. *Macromolecules* **2003**, *36*, 9451–9457.

(26) Silverstein, R. M.; Webster, F. X.; Kiemle, D. J., *Spectrometric Identification of organic compounds*. John Wiley & Sons: New York: 2005.

(27) Lim, C.; Hong, S.-I.; Kim, H. *J. Sol-Gel Sci. Technol.* **2007**, *43*, 35–40.

(28) Beamson, G.; Briggs, D., *High resolution XPS of organic polymers: the Scienta ESCA 300 database*; John Wiley & Sons Ltd: West Sussex, England, 1992.

(29) Brinker, C. J. *J. Non-Cryst. Solids* **1988**, *100*, 31–50.

(30) Pohl, E. R.; Osterholtz, F. D., *Molecular characterization of composite interfaces*; Plenum Press: New York, 1985.

(31) Iler, R. K., *The chemistry of silica: solubility, polymerization, colloid and surface properties, and biochemistry*; Wiley: New York, 1979.

(32) Hajji, P.; David, L.; Gerard, J. F.; Pascault, J. P.; Vigier, G. *J. Polym. Sci., Part B: Polym. Phys.* **1999**, *37*, 3172–3187.

(33) Brinker, C. J.; Keefer, K. D.; Schaefer, D. W.; Assink, R. A.; Kay, B. D.; Ashley, C. S. *J. Non-Cryst. Solids* **1984**, *63*, 45–59.

(34) Dzielawa, J.; Rubas, A.; Lubbers, C.; Stepinski, D.; Scurto, A.; Barrans, R.; Dietz, M.; Herlinger, A.; Brennecke, J. *Sep. Sci. Technol.* **2008**, *43*, 2520–2536.

(35) Kusuma, V. A.; Freeman, B. D.; Smith, S. L.; Heilman, A. L.; Kalika, D. S. *J. Membr. Sci.* **2010**, *359*, 25–36.